Mach 4 Performance of a Fixed-Geometry Hypersonic Inlet with Rectangular-to-Elliptical Shape Transition

Michael K. Smart and Carl A. Trexler
Hypersonic Airbreathing Propulsion Branch
NASA Langley Research Center
MS 168, Hampton, VA 23681.

Abstract

Wind-tunnel testing of a hypersonic inlet with rectangular-to-elliptical shape transition has been conducted at Mach 4.0. These tests were performed to investigate the starting and back-pressure limits of this fixed-geometry inlet at conditions well below the Mach 5.7 design point. Results showed that the inlet required side spillage holes in order to self-start at Mach 4.0. Once started, the inlet generated a compression ratio of 12.6, captured almost 80% of available air and withstood a back-pressure ratio of 30.3 relative to tunnel static pressure. The spillage penalty for self-starting was estimated to be 4% of available air. These experimental results, along with previous experimental results at Mach 6.2 (*Smart, M.K, "Experimental Testing of a Hypersonic Inlet with Rectangular-to-Elliptical Shape Transition", Journal of Propulsion and Power, Vol. 17, No. 2, pp 276-283, 2001)* indicate that fixed-geometry inlets with rectangular-to-elliptical shape transition are a viable configuration for airframe-integrated scramjets that operate over a significant Mach number range.

Nomenclature

A_{fm}	flow meter throat area
C_D	discharge coefficient for flow meter throat
m_c	mass capture ratio
p	pressure
x	distance along model

Subscripts

1	wind tunnel freestream
max	maximum back-pressure
ex	inlet exit
in	inside
out	outside
t2	Pitot
uns	unstart

Introduction

The design of inlets for hypersonic vehicles utilizing airframe integrated scramjet modules is a subject of interest in the high-speed propulsion community. In these configurations the vehicle bow shock performs the initial compression, and the capture shape of each scramjet module is required to be rectangular. Other requirements are that inlets will start at ramjet take-over speeds, operate over a large Mach number range, and be efficient during vehicle cruise. There is also a strong desire to have an intake with both fixed-geometry and no requirement for boundary layer bleed in order to reduce the overall mechanical complexity of the system. Another beneficial feature of a hypersonic inlet for some scramjet applications is a transition from a rectangular capture to an elliptical throat. The inlet may then be used in combination with an elliptical combustor, which is superior to a rectangular combustor in terms of the structural weight required to withstand a specified pressure/thermal load and the wetted surface area needed to enclose a specified cross-

sectional area. This type of configuration also reduces undesirable effects associated with hypersonic corner flows.

A number of three-dimensionally curved inlets leading to circular or elliptical combustors were designed and tested in the 1960's.[1-4] These fixed-geometry inlets performed well during wind tunnel tests and self-started with internal contraction ratios considerably above the one-dimensional theoretical starting limit first introduced by Kantrowitz and Donaldson[5]. Some recent work on three-dimensionally curved inlets has utilized streamline-tracing techniques to design high performance inlet configurations that includes a transition from a nearly-rectangular capture to an elliptical throat. A detailed methodology for the design of these fixed-geometry, rectangular-to-elliptical shape transition (REST) inlets was reported in Ref. 6. A description of the Mach 6.2 testing of a REST inlet with a design point of Mach 6.0 was reported in Ref. 7. The results of some computational analysis of these experiments was reported in Ref. 8.

Streamline tracing techniques are a commonly used method for the design of three-dimensionally curved inlets. These techniques utilize a pre-existing compressive flowfield and a chosen capture shape to construct an inviscid inlet surface from the flowfield streamlines that pass through the perimeter of the capture shape. Streamline traced inlets therefore have an inherent "design point" or "design Mach number" that is dictated by the original flowfield used to generate the inlet. The procedure is completed by making allowance for local boundary layer displacement thickness on the inlet surface. Operation of a well designed streamline traced inlet at its design point will nearly recreate the original internal flowfield. In this instance the inlet performance will be identical to the original flowfield, except for viscous losses at the walls and associated interactions. For scramjet applications, the design Mach number of a streamline traced inlet is usually chosen to be close to the maximum operational Mach number.

The REST inlet design procedure[6] is a quasi-streamtraced technique that makes use of multiple sets of streamlines to perform the required transition from a rectangular capture to an elliptical throat. The suitability of this procedure for the design of a Mach 6 scramjet inlet operating at conditions close to the design point has been experimentally verified[7]. This article describes an experimental investigation into the off-design performance of REST inlets. A key requirement for scramjet inlets is the ability to start at ramjet take-over speed. As the design point of a REST scramjet inlet will be well above this speed, an operational REST inlet must self-start and provide adequate compression at Mach numbers considerably below the design point. In an effort to examine these aspects of REST inlet performance, the current article focuses on the results of Mach 4 testing of a REST inlet with a design point of Mach 5.7.

Experimental Program

Wind Tunnel Test Conditions and Instrumentation

The experiments were conducted at NASA Langley Research Center in the Mach 4 Blown Down Facility (M4BDF). Typical operating conditions were a Mach number of 4.03, a stagnation pressure of 200 psia (1.38 Mpa), a stagnation temperature of 522° R (290 K), and a Reynolds number of 20×10^6/ft (6.1×10^6/m). The M4BDF has a 9in. x 9in. (22.9cm x 22.9cm) test section which is 3ft (0.91m) in length. Diagnostic instrumentation for the tests included 41 surface pressure taps, an 8 probe Pitot rake at the exit of the inlet, a thermocouple to monitor the model temperature, and a Schlieren system for visualization of the external flow. The mass flow rate through

the inlet was determined using a sonic throat based flow metering device. All data was acquired and saved using a PC based data acquisition system, and typical runs lasted approximately 2 minutes.

Inlet Model

Figure 1 shows a photograph of the inlet installed in the wind tunnel test section. The model was manufactured at NASA Langley using a stereo-lithography technique. This method enabled the three-dimensional internal inlet shape to be manufactured for a approximately 1/10 of the cost of an aluminium model. The epoxy model produced with this technique had 0.025" radius leading edges, and was able to withstand conditions in the M4BDF test section with the addition of fiberglass reinforcement on the external cowl surface.

The inlet model had a total length of 14.27 in., with cowl closure 8.95 in. from its most forward point, the throat 12.52 in. from its most forward point, and a 1.75 in. elliptical isolator downstream of the throat. The capture area of 4.55 in^2 was 3.0 in. wide and the 100% capture mass flow rate for the inlet was 1.92 lb/s. Figure 2 shows a schematic of the nominal streamlines along which surface pressure taps were distributed. Internal pressure taps were concentrated on one side of the model (as the model had a vertical plane of symmetry) and were placed on the six streamlines (labeled A, C, D, E, G and H in Fig. 2) at 8 different axial stations along the inlet. Two extra taps were added at the exit (B and F in Fig.2) and a solitary external pressure tap was included just downstream of cowl closure in order to monitor inlet spillage prior to unstart. Figure 3 shows the positions of the Pitot probes at the inlet exit. The vertical plane of symmetry and use of adjacent surface pressure taps enabled the exit flow to be mapped in some detail with only 8 probes.

Flow Meter Calibration

The flow metering device used for the current experiments was calibrated for operation in the range of 0.75 to 1.60 lb/s. Figure 4 shows the discharge coefficient values measured during calibration and the linear fit for C_D used to calculate inlet mass capture in the current test program.

Inlet Geometry

The REST inlet model used in the test program was an improved version of that tested at Mach 6.2[7]. Changes to the previous shape were based on experience gained during the Mach 6.2 test program and the requirement for self-starting at Mach 4.0. These entailed:

1. Slight reduction of the design point to Mach 5.7.
2. A 20% reduction in inlet length (as a result of a less conservative boundary layer separation criterion).
3. Cut-back of the cowl to allow more flow spillage and a reduced internal contraction ratio.

These changes resulted in an inlet with an overall geometric contraction ratio of 4.80 and an internal contraction ratio of 1.77.

The previous REST inlet self-started at Mach 6.2 with an internal contraction ratio of 2.15, which is well above the Kantrowitz starting limit[5] at these conditions. Reduction of the internal contraction ratio to 1.77 in the current inlet was hoped to be satisfactory for self-starting at Mach 4, however, inlet start-ability is notoriously unpredictable. For this reason, space was provided for the addition of "spill" holes on the sides and cowl of the inlet between cowl closure and the throat. When initial tests indicated that the inlet would not self-start, numerous 1/8" diameter holes directed at 45° to the downstream direction of the local surface were drilled in these areas. Figure 5 shows a close-up view of some of these holes, which were able to be filled and

re-opened as required. These holes constituted a passive system for spilling enough mass to allow the inlet to self-start. They also spilled at a reduced level once the inlet was started. This inlet starting technique has considerable system level advantages over more elaborate methods involving variable geometry or active bodyside bleed systems.

Experimental Results

The goals of the experimental program were two-fold; (1) to ascertain whether the as-designed inlet would self-start at Mach 4, and if not, how many spill holes would be needed for self-starting; and (2) to characterize the performance and back-pressure limits of a REST inlet at Mach numbers well below the design point. Initial tests showed that the inlet did require spill holes in order to start at Mach 4. After considerable testing of different spillage configurations (varying the number, axial position, and circumferential position of holes), it was found that holes on the side of the inlet were most effective, and a minimum of 16 holes (8 on each side) were required for self-starting.

Characteristics of Self-Starting Inlet Configurations

Figure 6 shows the time history of the flow meter throat area (A_{fm}), the mass capture ratio (m_c), and the symmetry plane pressure taps located inside (p_{in}) and outside (p_{out}) the cowl (just downstream of cowl closure). This particular data is for the self-starting configuration with 30 side holes. In this run the inlet started with the tunnel at t = 0 seconds with the flow meter fully opened. As A_{fm} was gradually decreased the inlet experienced an increasing back-pressure level until unstart occurred at approximately t = 86 seconds. Unstart is indicated in Fig. 6 by an instantaneous drop in m_c and an accompanying change in both p_{in} and p_{out}. Subsequent increase of A_{fm} reduced the applied back-pressure, and the inlet was observed to restart at approximately t = 98 seconds. Restart of an inlet after such a mechanically imposed unstart is proof of its ability to self-start at these inflow conditions.

Another feature of the inlet shown in Fig. 6 is the decrease in m_c observed prior to unstart. This particular configuration had a started mass capture ratio of $m_c = 0.763$. Just before unstart, however, m_c reduced to 0.715. As both p_{in} and p_{out} remained unchanged until the inlet unstart, no pre-unstart spillage occurred in front of the cowl. The reduced mass capture was solely due to increased spillage through the "starting" holes as the back-pressure level increased inside the inlet. The wall thermocouple measurements (not shown) indicated that the model reached adiabatic wall conditions early in the run, and remained at this temperature throughout.

Figure 7 shows a schlieren image of a typical test when the inlet was started. Flow is from left to right and the steady external shock structure above the inlet contained initial waves from the leading edges of the inlet, a second wave emanating from the lower or bodyside leading edge, and finally the shock emanating from the point of cowl closure. Numerous other waves can be detected in the image, some of which are generated by the external pressure tubing. Figure 8 shows an instantaneous schlieren image of the unsteady flowfield that occurred after unstart. In this instance the cowl closure shock of the started flowfield is replaced by a shock of higher strength that oscillates slightly upstream of cowl closure. The remainder of the external shock structure appeared identical to that observed when the inlet was started (Fig. 7).

Figure 9 shows the normalized pressure distributions along instrumentation streamlines A, C, D, E, G and H for the minimum spillage configuration (16 side

holes) during tare operation; i.e. no back-pressure. The pressure levels on each streamline increased gradually up to cowl closure, indicating that all surfaces are contributing to the compression. The internal flow downstream of cowl closure was dominated by the three-dimensional cowl shock that reflected multiple times before the inlet exit. The close correlation between the pressure distributions on streamlines D and H confirmed that the flow is nearly symmetric. The tare mass capture ratio for this minimum spillage configuration was $m_c = 0.797$, and the average compression ratio at the inlet exit was $p_{ex}/p_1 = 12.60$.

The bodyside pressure distributions (streamline A) for the minimum spillage configuration during tare operation, maximum back-pressure and after unstart are shown in Fig. 10. The tare pressure distribution shows gradual pressure rise upstream of cowl closure and the effect of cowl shock reflections downstream of cowl closure. The maximum back-pressure plot displays upstream influence well beyond the inlet throat and a maximum back-pressure ratio at the inlet exit of $p_{max}/p_1 = 30.29$. This is a factor of 2.40 greater than the tare compression ratio for this configuration. The unstarted flowfield influenced all but the most forward bodyside pressure tap, and led to a reduction in mass capture ratio to $m_c = 0.59$. The unstarted plot also shows a back-pressure level of $p_{uns}/p_1 = 27.5$ at the inlet exit, which is approximately 90% of the maximum back-pressure. This form of "soft" unstart is more typical of inlets with considerably lower internal contraction ratios, and is postulated to be caused by the presence of the spillage holes.

Figures 11a and b display the normalized Pitot pressure distributions along horizontal and vertical branches of the Pitot rake at the inlet exit. Included in the figures are the tare, maximum back-pressure and unstart distributions for the minimum spillage configuration. During tare operation the horizontal Pitot distribution (Fig. 11a) was constant through the core of the exit flow at a value of $p_{t2}/p_1 \sim 89$. At maximum back-pressure the distribution included local maxima ($p_{t2}/p_1 \sim 77$) on either side of the central region which dropped to a level of $p_{t2}/p_1 \sim 62$. Once the inlet unstarted the Pitot pressure dropped by a considerable margin, except at the center of the span where it remained at the same level as at the maximum back-pressure condition.

The vertical Pitot distribution (Fig. 11b) for tare operation peaked at the center of the inlet exit at $p_{t2}/p_1 \sim 89$. Pitot pressure remained at a high level on the cowlside of the span, while decreasing more quickly on the bodyside. This feature was also observed in the previous Mach 6 experiments.[7] At maximum back-pressure the Pitot distribution was significantly transformed. In this instance the flow separated into two distinct regions; (1) a cowlside region with high Pitot levels that peaked at $p_{t2}/p_1 \sim 108$ (well above the maximum observed during tare operation), and (2) a bodyside region which had very low Pitot levels not much greater than the bodyside wall pressure. This type of Pitot distribution is consistent with computational solutions of the back-pressured Mach 6 REST inlet that were reported in Ref. 8. These solutions indicated a flowfield containing an asymmetric shock train on the cowlside of the inlet, with highly distorted flow adjacent to the bodyside. The vertical Pitot distribution for the unstarted flow showed highest levels on the cowlside, reaching a maximum of $p_{t2}/p_1 \sim 72$ near the cowl.

Self-starting configurations with up to 40 spill holes (20 on the cowl; 10 on each side) were tested in the program. Mass capture values varied between m_c=0.758 for the 40 hole configuration to m_c=0.797 for the minimum spillage configuration with 16 holes (8 on each side). The inlet compression

ratio, determined from the average of the 8 surface pressure taps at the exit of the inlet during tare operation, ranged between p_{ex}/p_1 = 11.7 and 13.5 for all configurations. The maximum back-pressure ratio, determined from the average of the exit pressure taps at the point of maximum back-pressure, remained relatively constant for all configurations, varying between p_{max}/p_1 = 29.8 and 31.5. These inlet performance parameters compare favorably with those obtained from other hypersonic inlet configurations operating at Mach 4. These test results supply some measure of confidence in the ability of REST inlet configurations to operate effectively at conditions well below the design point.

Effect of Spillage Hole on Started Mass Capture

As the test program progressed it became clear that spillage holes on the cowl were far less effective than spillage holes on the side for improving inlet start-ability. For example, a configuration with 16 side holes was found to self-start, but a configuration with 10 side holes and 20 cowl holes would not. In this case an extra 6 side holes moved the inlet more towards self-starting than the addition of 20 cowl holes. It is postulated that this difference is due to the thicker boundary layer on the sides of the inlet relative to the boundary layer on the cowl. The greater the proportion of boundary layer fluid that is spilled, the higher is the average total pressure of the remainder of the air that must pass through the inlet throat, and the more effective the spillage is in improving start-ability. The greater thickness of the side wall boundary layer (relative to the thickness of the cowl boundary layer) is expected to lead to a higher proportion of boundary layer spillage through side holes, and greater effectiveness of side holes for improving start-ability.

The holes continued to spill after the inlet configuration was started, albeit at a reduced level. The started spillage losses of both the side and cowl holes were quantified by examining two separate groupings of the data; (1) with the number of side holes constant, and (2) with the number of side holes constant. Figure 12a shows a plot of started inlet mass capture versus the number of cowl holes present, for all configurations with 20 side holes. The data shows a relatively linear decrease in m_c with the addition of more cowl holes, and a linear fit to the data indicates a reduction of 0.171% in m_c for each cowl hole. Figure 12b shows a plot of started m_c versus the number of side holes present for all configurations with no cowl holes. A linear fit to this data indicated a reduction of 0.254% in m_c for each side hole. Based on this level of spillage, the penalty for enabling the current inlet configuration to self-start is a 4 % reduction in the mass capture of the inlet.

Conclusions

Results of Mach 4 wind tunnel testing of a fixed-geometry hypersonic inlet were reported. The tested quasi-streamline traced inlet had a geometric contraction ratio of 4.80, an internal contraction ratio of 1.77 and a Mach 5.7 design point. It also included a transition from a nearly rectangular capture to an elliptical throat. The tests were conducted to determine the performance and starting limits of the inlet at ramjet/scramjet take-over speeds.

Initial testing of the inlet indicated that it would not self-start at Mach 4. This limitation was overcome by the introduction of spillage holes on the cowl or sides of the inlet between cowl closure and the inlet throat. Numerous spillage hole configurations were examined during the test program, and it was observed that holes on the sides of the inlet were more effective than holes on the cowl for improving inlet start-

ability. It was postulated that this was due to side holes spilling a larger proportion of boundary layer fluid than cowl holes. The self-starting configuration with minimum spillage included a total of 16 holes, 8 on each side of the inlet. Once started, this configuration generated a compression ratio of 12.6, captured 79.7% of the available air and withstood a mechanically imposed back-pressure ratio of 30.3 relative to the tunnel static pressure. The started spillage loss due to the presence of the holes was estimated to be 4% of the available air.

These experiments show that good performance is obtainable from streamline traced inlet configurations at Mach numbers well below the design point. In conjunction with the previous experiments at on-design conditions[7], the current results indicate that fixed-geometry inlets with rectangular-to-elliptical shape transition are a viable configuration for airframe-integrated scramjets that operate over a significant Mach number range.

Acknowledgements

The first author wishes to thank Mark Cagle of the Model Systems Branch at NASA Langley Research Center for his help with the design and fabrication of the model.

References

[1]Hartill, W.B., "Analytical and Experimental Investigation of a Scramjet Inlet of Quadriform Shape", Tech Rep. AFAPL-TR-65-74, U.S. Air Force, August 1965, The Marquardt Corporation.

[2]Billig, F.S., "Supersonic Combustion Ramjet Missile", Journal of Propulsion and Power, Vol. 11, No. 6, pp 1139-1146, 1995.

[3]Kutshenreuter, P.H., "Hypersonic Inlet Tests in Helium and Air", General Electric Company Advanced Engine and Technology Departments, Cincinnati, Ohio; Presented at the AIAA Propulsion Joint Specialist Conference, The United States Air Force Academy, Colorado, June 14-18, 1965.

[4]Molder, S., and Romeskie, J.M., "Modular Hypersonic Inlets with Conical Flow", AGARD Conference Proceedings No. 30, 1968.

[5]Kantrowitz, A. and Donaldson, C., "Preliminary Investigation of Supersonic Diffusers", NACA ACR No. L5D20, 1945.

[6]Smart, M.K., "Design of Three-Dimensional Hypersonic Inlets with Rectangular-to-Elliptical Shape Transition", Journal of Propulsion and Power, Vol. 15, No. 3, pp 408-416, 1999.

[7]Smart, M.K., "Experimental Testing of a Hypersonic Inlet with Rectangular-to-Elliptical Shape Transition", Journal of Propulsion and Power, Vol. 17, No. 2, pp 276-283, 2001.

[8]Smart, M.K. and White, J.A., "Computational Investigation of the Performance and Back-Pressure Limits of a Hypersonic Inlet", AIAA paper 2002-0508, January 2002.

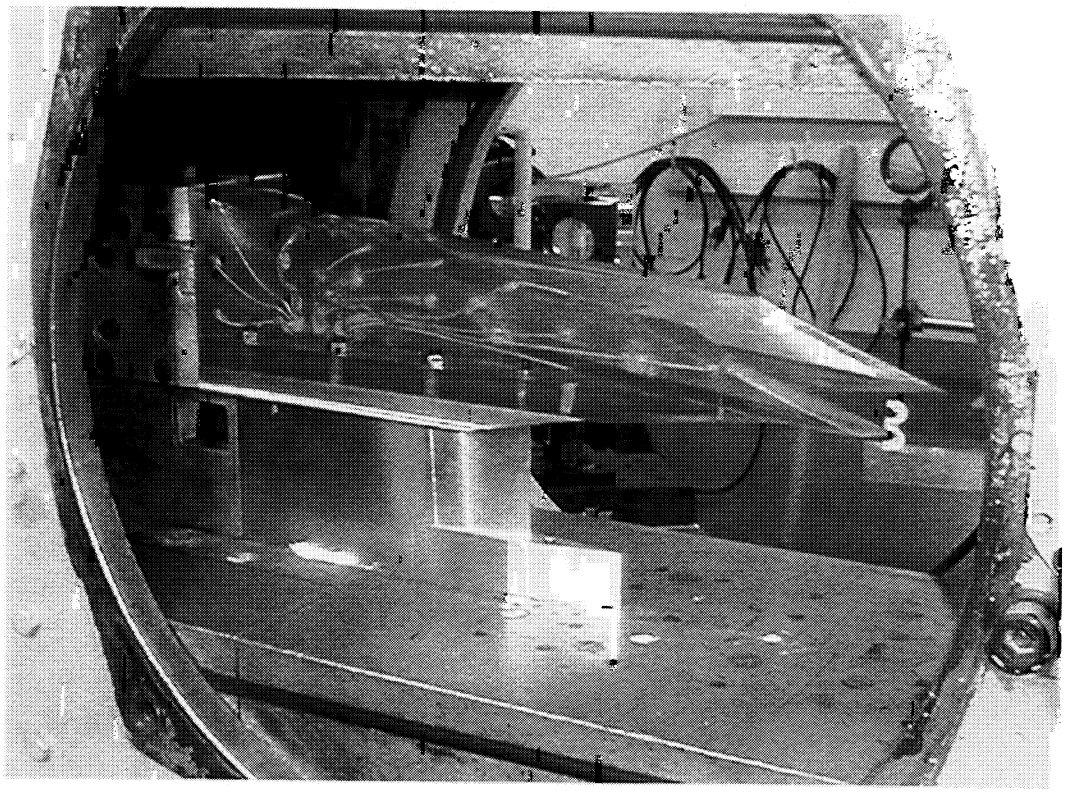

Figure 1 - REST inlet installed in the M4BDF.

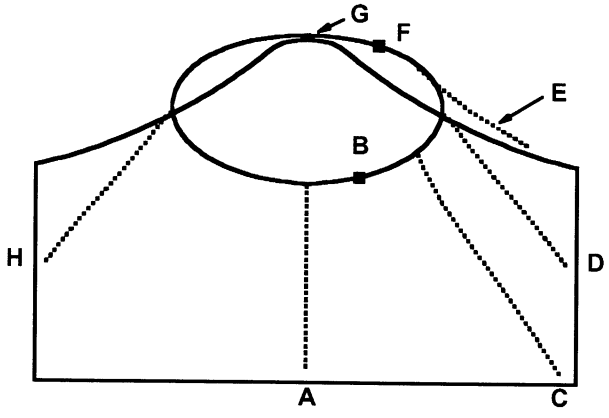

Figure 2 - Schematic of the instrumentation streamlines.

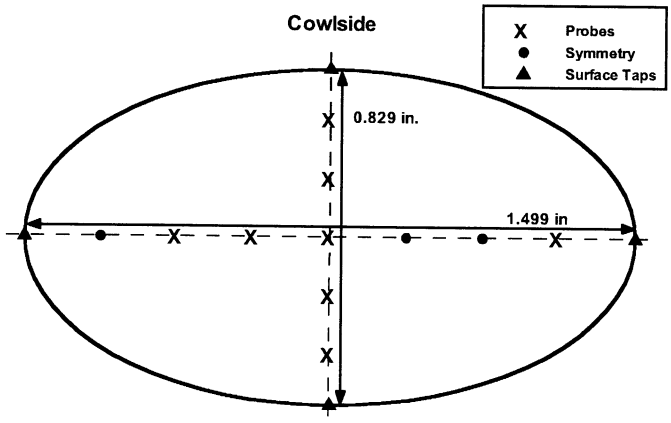

Figure 3 – Schematic of Pitot probe positions.

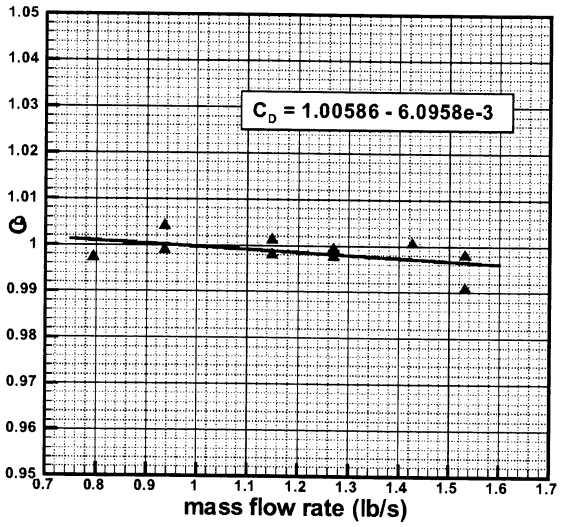

Figure 4 - Flow meter calibration data.

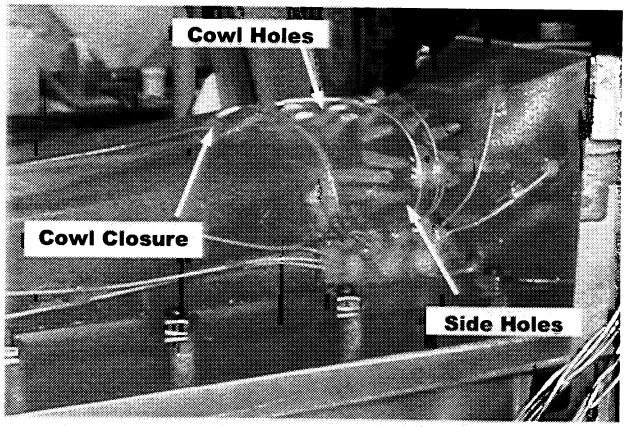

Figure 5 – Close-up view of inlet spillage holes.

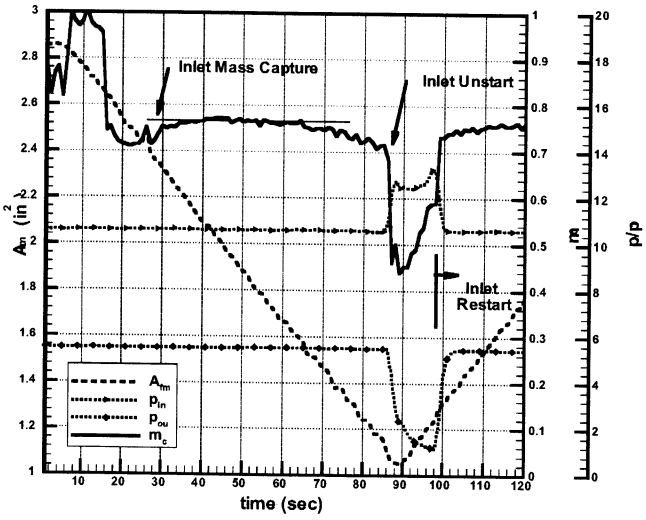

Figure 6 - Plot of key parameters during a run with the 30 side hole configuration.

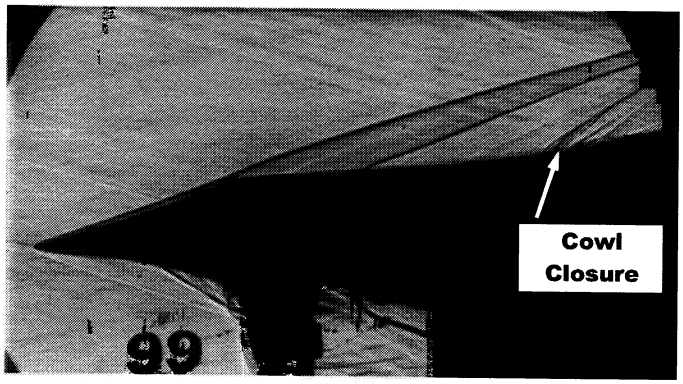

Figure 7 - Schlieren image of the started flowfield of the minimum spillage configuration .

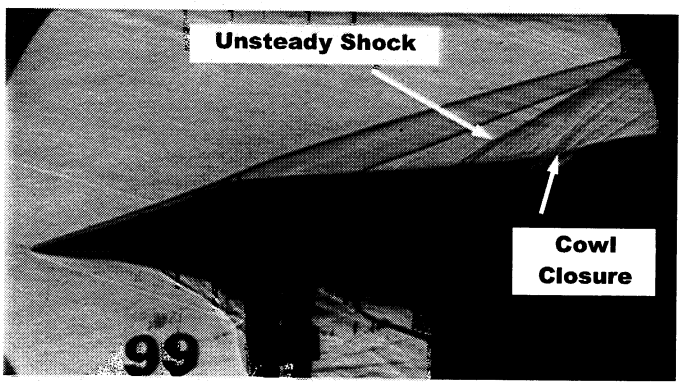

Figure 8 - Instantaneous schlieren image of the unstartd flowfield of the minimum spillage configuration.

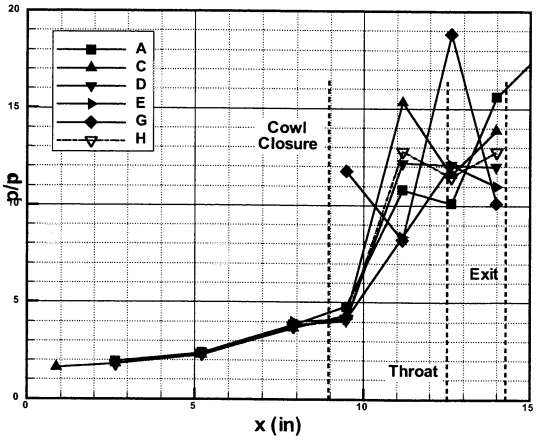

Figure 9 - Surface pressure distribution for tare operation.

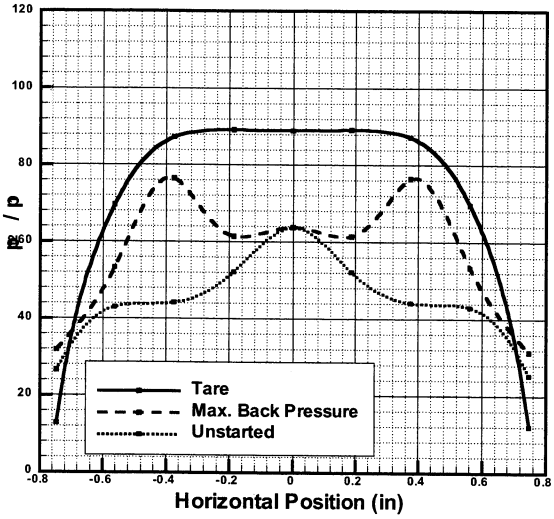

Figure 11a - Horizontal Pitot distributions at the inlet exit.

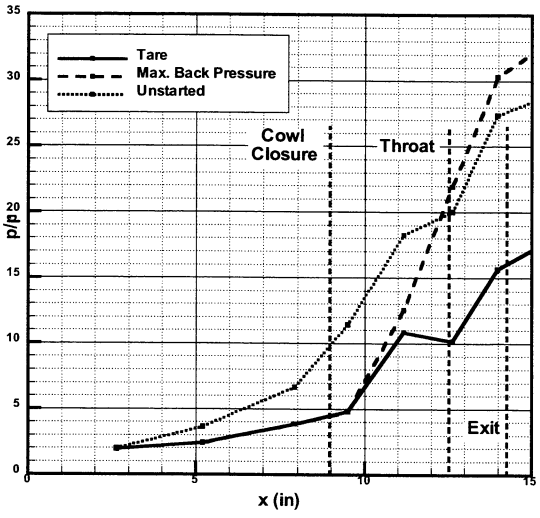

Figure 10 - Bodyside pressure distributions at different stages of a test.

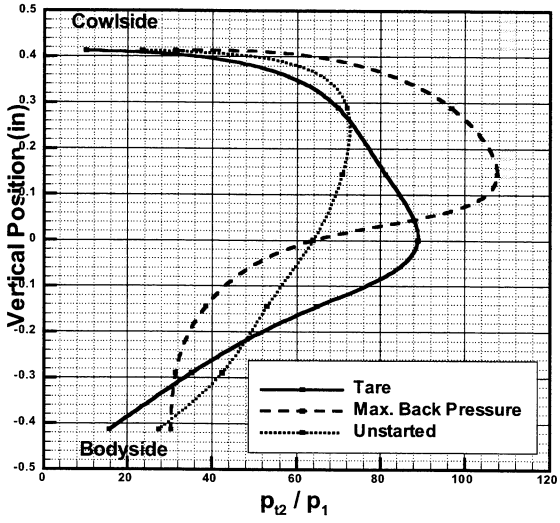

Figure 11b - Vertical Pitot distributions at the inlet exit.

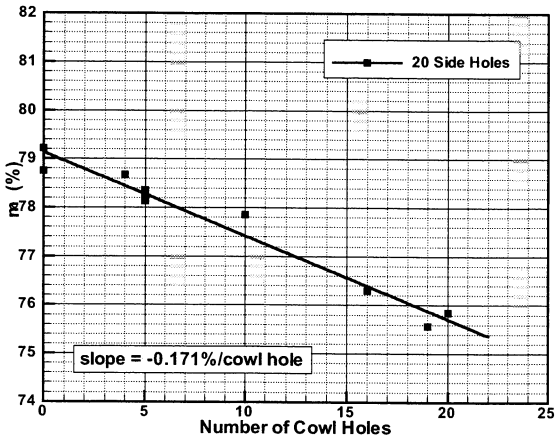

Figure 12a - Started mass capture variation with number of cowl holes.

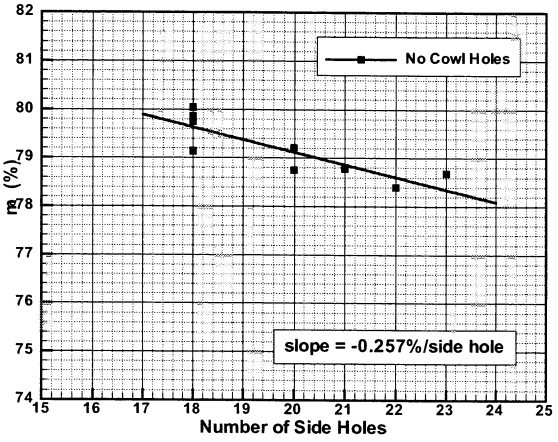

Figure 12b - Started mass capture variation with number of side holes.